Becoming a new neuron in the adult olfactory bulb

Alan Carleton[1], Leopoldo T. Petreanu[2], Rusty Lansford[3], Arturo Alvarez-Buylla[4] and Pierre-Marie Lledo[1]

[1] *Pasteur Institute, Laboratory of Perception and Memory, CNRS UMR 2182, 25 Rue du Dr Roux, 75015 Paris, France*

[2] *The Rockefeller University, 1230 York Avenue, New York, New York 10021, USA*

[3] *Division of Biology, Biological Imaging Center, Beckman Institute, California Institute of Technology, Pasadena, California 91125, USA*

[4] *Neurosurgery Research, UCSF, San Francisco, California 94134, USA*

Correspondence should be addressed to P.-M.L. (pmlledo@pasteur.fr)

Published online 21 April 2003; doi:10.1038/nn1048

New neurons are continually recruited throughout adulthood in certain regions of the adult mammalian brain. How these cells mature and integrate into preexisting functional circuits remains unknown. Here we describe the physiological properties of newborn olfactory bulb interneurons at five different stages of their maturation in adult mice. Patch-clamp recordings were obtained from tangentially and radially migrating young neurons and from neurons in three subsequent maturation stages. Tangentially migrating neurons expressed extrasynaptic $GABA_A$ receptors and then AMPA receptors, before NMDA receptors appeared in radially migrating neurons. Spontaneous synaptic activity emerged soon after migration was complete, and spiking activity was the last characteristic to be acquired. This delayed excitability is unique to cells born in the adult and may protect circuits from uncontrolled neurotransmitter release and neural network disruption. Our results show that newly born cells recruited into the olfactory bulb become neurons, and a unique sequence of events leads to their functional integration.

© 2003 Nature Publishing Group http://www.nature.com/natureneuroscience

Neurons continue to be generated in the adult vertebrate brain[1,2]. In contrast to the function of neurons born during development, new neurons in the adult brain continually replace older ones within mature circuits[2,3]. The function of neuronal replacement in adult mammals remains poorly understood, however. In the adult mammalian forebrain, the subventricular zone (SVZ) of the lateral ventricles contains the largest pool of neural stem cells that continually generate neurons in adult life[1]. In a process that begins in the embryo[4] and continues postnatally[5] and into adult life[6], SVZ stem cells give rise to neuroblasts that migrate tangentially along the rostral migratory stream (RMS) up to the olfactory bulb (OB) where they migrate radially to complete their differentiation into neurons. The new cells have morphological characteristics of granule and periglomerular cells[5,7,8] and express neuronal markers[9,10]. To date, however, there is no direct electrophysiological evidence that the new bulbar cells are functionally integrated or fire action potentials. Such information would be important, not only to conclusively identify new cells as neurons but also to understand how they contribute to the function of adult brain circuits[2,3,11].

Interneurons in the OB have an essential role in shaping the olfactory information that reaches the olfactory cortex. Dendrodendritic synapses between mitral and granule cells (GCs) are important sites of plasticity for the processing of olfactory information[12]. As adult-generated cells born in the SVZ differentiate into bulbar interneurons, newborn neurons probably contribute to essential aspects of olfactory processing. Although modeling and experimental studies have already provided evidence for a role of newborn GCs in olfactory discrimination[13,14], physiological data indicating the functional contribution of new neurons to the adult OB are still lacking. For example, whereas much work has been devoted to understanding the birth and migration mechanisms of new SVZ neuroblasts[1], no information is available concerning the temporal sequence of electrophysiological changes that new neurons undergo. Such information is essential to understand how newly generated neurons become functionally integrated into adult neural networks.

This gap in knowledge is due, in part, to difficulty in distinguishing newborn cells from older ones in living brain tissues. Using a replication-defective retrovirus expressing alkaline phosphatase, five morphological stages in the maturation of new bulbar GCs have been described[10]. Here we used a retrovirus that carries enhanced green fluorescent protein (eGFP), which allowed us to characterize the electrophysiological properties of newborn OB interneurons at different stages of maturation in adult living brain tissue. We describe how membrane properties and synaptic activities change during their morphological maturation. Our work provides evidence that newborn adult neurons do not simply recapitulate normal developmental patterns of maturation, but rather have unique properties likely related to their integration into fully assembled adult neural circuits.

Results

Live imaging of the maturation of newborn interneurons

A replication-defective retrovirus expressing eGFP–GAP43 was injected into the ventricle to label neuronal precursors in the SVZ of adult mice (**Fig. 1a**). Between 6 and 47 days later, GFP^+ cells were recorded from OB slices. The eGFP–GAP43 construct

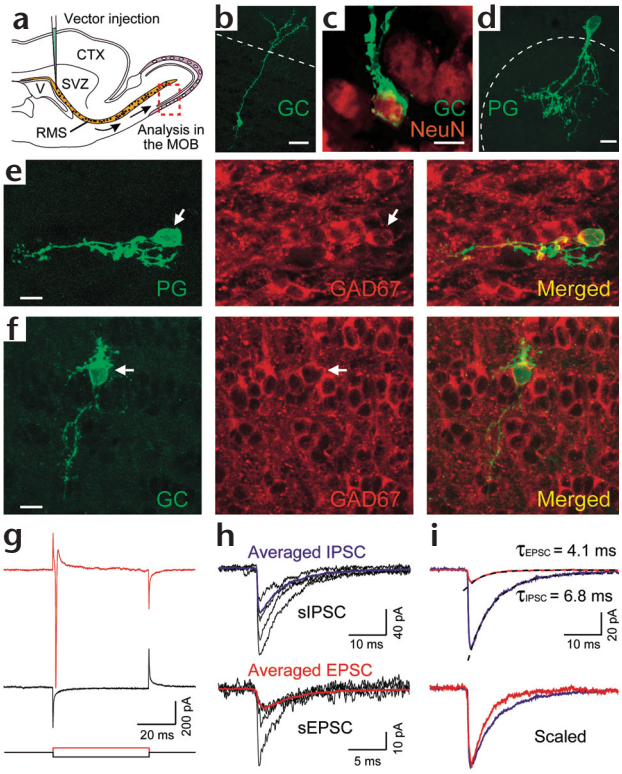

Fig. 1. Newborn neurons are functionally integrated into the adult olfactory bulb. (**a**) Experimental procedure. The retroviral vector was injected stereotaxically in the subventricular zone (SVZ). Infected neuroblasts expressed eGFP and migrated along the rostral migratory stream (RMS) into the main OB (MOB). CTX, cortex; V, lateral ventricle. (**b**, **c**) Example of a newly generated GC. The GFP$^+$ cell (**b**) expressed the nuclear neuronal marker NeuN (**c**). Scale bars, 25 and 6 μm for **b** and **c**, respectively. The dotted line in **b** delineates the mitral cell layer. (**d**) Example of a newly generated periglomerular cell (PG). The dotted line depicts the glomerulus. Scale bar, 7 μm. (**e**, **f**) White arrows point to a newborn PG (**e**) and a newborn GC (**f**) which both express GAD67. Scale bars, 7 μm. (**g**–**i**) Patch-clamp recordings of a newborn PG cell showing properties of neurons and functional integration into the OB (holding potential of –60 mV). (**g**) A 20-mV depolarizing step evoked a fast inward Na^+ current (red trace). (**h**) Pharmacological analysis revealed the presence of sIPSCs mediated by $GABA_A$ receptor activation (top, single events in black and average of 40 events in purple) and of sEPSCs mediated by AMPAR activation (bottom, average of 40 events in red). (**i**) The averaged sIPSC and sEPSC shown in **h** are superimposed (top) and scaled (bottom) for time course comparison. Decay times were fitted using a single exponential (dotted lines).

targeted the transduced protein to the plasma membrane[15], which stained the entire surface of the newborn cells, thus revealing precisely stage-specific morphology without further tissue processing (**Fig. 1b–f**). As previously reported[10], the population of labeled GCs can be divided into five different classes according to their morphology and location: class 1, migrating neuroblasts in the rostral extension of the RMS (**Fig. 2a**); class 2, radially migrating neuroblasts in the GC layer (**Fig. 2f**); class 3, maturing GCs with growing dendritic processes that do not extend beyond the mitral cell layer (**Fig. 3a**); class 4, GCs with dendritic arborization in the external plexiform layer (EPL) and almost devoid of spines (**Fig. 3d**); and class 5, mature GCs with complex dendritic arborization and spines (**Fig. 4a**).

GFP$^+$ neuroblasts with a migratory morphology were observed in the core of the OB 6 days after virus injection. By 14 days post-injection, many GFP$^+$ cells had attained a fully mature morphology, including well-developed dendritic arbors in the EPL with many spines. Consistent with previous reports[5,6,8], a smaller number of these labeled neurons were also seen in the glomerular layer (**Fig. 1d** and **e**) and corresponded to newly formed periglomerular neurons.

Newborn neurons integrate into adult OB

GFP$^+$ mature GCs (class 5) and periglomerular cells both expressed neuronal markers as revealed by colocalization of virally encoded eGFP with NeuN (**Fig. 1c**) and GAD67, an enzyme required for the biosynthesis of GABA (**Fig. 1e** and **f**). Whereas their morphology, synaptic contacts and molecular markers strongly suggested that the newly formed cells corresponded to neurons, there was no direct electrophysiological evidence supporting their functional maturity and integration into the OB network. To investigate whether newborn cells were functional, GFP$^+$ neurons with a mature morphology were recorded using the patch-clamp technique, 3–5 weeks after viral infection (n = 13). We could ascertain that recorded cells corresponded to newborn cells because GFP, detected by fluorescence microscopy, entered into the patch pipette upon starting the whole-cell configuration. In addition, a red fluorescent dye included in the pipette medium diffused into the recorded cells, allowing unambiguous identification (**Fig. 4b** and **c**).

An example of periglomerular cell recording 4 weeks after viral infection is presented in **Fig. 1g–i**. A fast tetrodotoxin (TTX)-sensitive voltage-gated Na^+ current (**Fig. 1g**), characteristic of mature neurons, was observed in all tested cells (n = 13). In addition, recorded GFP$^+$ mature bulbar interneurons also displayed GABAergic and glutamatergic spontaneous synaptic events, indicating a functional integration into the OB circuit (n = 13; **Fig. 1h** and **i**). This is the first direct electrophysiological evidence that newly formed interneurons in the adult OB become mature and functionally integrated. As seen in other brain regions[11,16–18], physiological evidence shows that newborn cells correspond to mature neurons. Because the new OB neurons undergo a series of changes during their migration in the RMS and OB, we investigated their physiological characteristics at different stages of maturation. Most SVZ progenitors give rise to new neurons in the GC layer; we therefore concentrated our study on this population and recorded from more than 150 labeled cells taken from all stages.

Electrophysiological properties of migrating neurons

Whole-cell recordings were obtained from tangentially migrating class-1 GFP$^+$ cells in the RMS and radially migrating class-2 cells in the GC layer of the OB. From voltage-clamp recordings, we first extracted passive membrane properties such as the input membrane resistance (R_m), the cell membrane capacitance (C_m) and the resting membrane potential (V_{rest}). Class-1 (**Fig. 2a–e**) and class-2 neurons (**Fig. 2f** and **g**) showed membrane properties of immature neuronal precursors. Using a K^+-based electrode solution, the average V_{rest} was –37.1 ± 2.6 mV (mean ± s.e.m., n = 26) and –46.2 ± 2.7 mV (n = 23) for classes 1 and 2, respectively. Both cell types had relatively high R_m values (2.02 ± 0.21 GΩ, n = 21 and 1.99 ± 0.22 GΩ, n = 23 for classes 1 and 2, respectively). In agreement with high R_m values, these cells were characterized by a complete lack of voltage-gated Na^+ conductance (0/27 and

© 2003 Nature Publishing Group http://www.nature.com/natureneuroscience

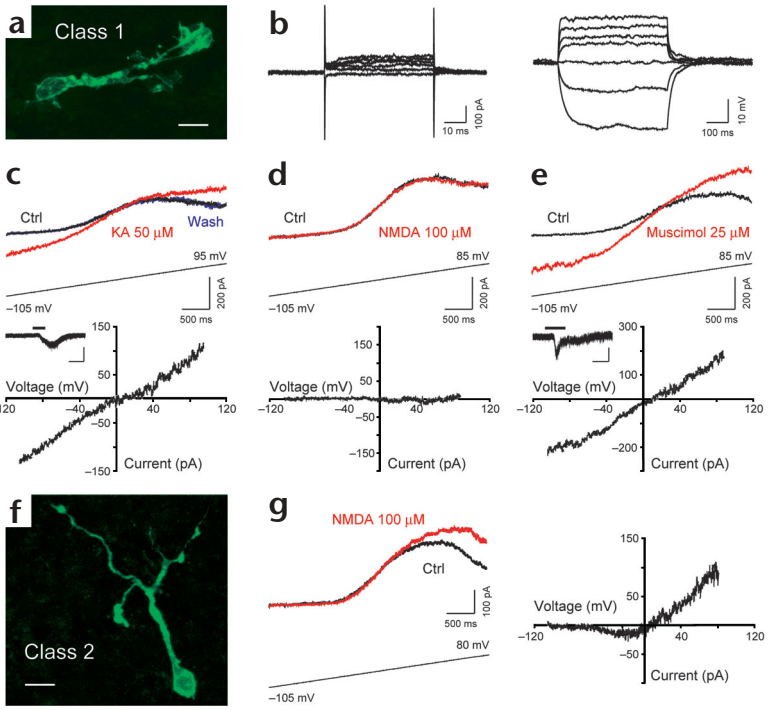

Fig. 2. Functional properties of class-1 and class-2 newborn granule cells. (**a**–**e**) Electrophysiological properties of a typical class-1 cell. (**b**) The cell in **a** showed neither Na^+ currents during voltage-clamp (left traces) nor spikes during current-clamp (right traces). (**c**–**e**) *I*–*V* relationships have been constructed from measurements made in the presence of receptor agonists during depolarizing ramps. (**c**) AMPAR-mediated currents recorded in the same cell as in **b**. The responses to a depolarizing ramp are shown (top traces) under control conditions (black trace; TTX 1 μM, BMI 20 μM and cyclothiazide 100 μM), during kainate application (red trace) and after washout (purple trace). The corresponding *I*–*V* curve is shown in the bottom panel. The inset shows the current generated by kainate application (50 μM, thick bar) on the same cell (scale bars, 50 s and 100 pA). (**d**) Absence of NMDAR-mediated response (top traces) under control conditions (black trace; TTX 1 μM, NBQX 10 μM and D-serine 50 μM) and during NMDA application (red trace). (**e**) $GABA_A$ receptor–mediated currents recorded from the same cell as in **d** in control bath solution (black trace, same medium as in **d**) and during muscimol treatment (red trace). The corresponding *I*–*V* curve is shown in the bottom panel, and the inset shows the current generated by bath application of muscimol 25 μM (thick bar) on another cell. Scale bars, 50 s and 50 pA. (**f**, **g**) A class-2 neuron (depicted in **f**, scale bar 10 μm) showed similar physiological properties as class-1 cells except that it expressed functional NMDARs. (**g**) The responses to a depolarizing ramp are shown (left traces) in control bath solution (black trace, TTX 1 μM, BMI 20 μM, NBQX 10 μM and D-serine 25 μM) and during NMDA treatment (red trace). The corresponding *I*–*V* curve is shown on the right. All neurons were held at –60 mV.

0/31 tested cells from classes 1 and 2, respectively; **Fig. 2b**). Depolarizing voltage steps revealed only voltage-gated K^+ currents. The absence of Na^+ current was consistent with the inability to generate action potentials in current-clamp (**Fig. 2b**). These properties are similar to those associated with precursor cells isolated from adult brain SVZ[19,20].

We next studied whether GFP^+ migrating young cells show extrasynaptic neurotransmitter receptors and/or synaptic events. Class-1 and class-2 neurons never showed spontaneous postsynaptic currents (sPSCs) during prolonged recording times (up to 15 min; 0/26 and 0/30 tested cells for stages 1 and 2, respectively; data not shown). To determine whether the lack of synaptic event resulted from the absence of functional receptors, we bath-applied different agonists of ionotropic receptors. Addition of kainate (50 μM), a non-selective agonist of both AMPA and kainate receptors, induced an inward current in some class-1 (**Fig. 2c**; 29%, $n = 14$) and most class-2 neurons (71%, $n = 17$). This response was reversible and reproducible. In the presence of TTX (1 μM) and the $GABA_A$ receptor antagonist BMI (20 μM), the mean kainate-induced current was –27.5 ± 8.3 pA ($n = 4$, **Fig. 2c**) and –54.3 ± 20.3 pA ($n = 12$) for classes 1 and 2, respectively. In internal medium containing polyamine (Methods), Ca^{2+}-permeable AMPA receptors (AMPARs) showed inwardly rectifying current–voltage (*I*–*V*) relationships, whereas Ca^{2+}-impermeable AMPARs showed nearly linear *I*–*V* curves. The linear AMPAR-mediated response obtained in **Fig. 2c** indicates that AMPARs expressed in immature cells are Ca^{2+}-impermeable and thus contain the GluR2 subunit.

Addition of cyclothiazide (100–200 μM), a selective antagonist of AMPAR desensitization, did not reveal any AMPA/kainate response in cells that lacked such a response ($n = 6$, data not shown). In cells responding to kainate, however, bath application of cyclothiazide significantly increased the response (from –32.4 ± 7.9 to –70.2 ± 12.2 pA, $n = 5$; Wilcoxon pairs test, $P < 0.05$). In agreement with this, 1 μM NBQX completely antagonized the kainate-induced current ($n = 5$, data not shown). We conclude that functional AMPARs are present in a small fraction of class-1 neuroblasts and in the majority of class-2 cells.

To examine whether GFP^+ neurons express NMDA receptors (NMDARs), NMDA (100–200 μM) was added in Mg^{2+}-containing medium in the presence of 1 μM TTX, 25–50 μM D-serine, 20 μM BMI and 10 μM NBQX. Cells were depolarized by voltage ramps from –105 to +80 mV to remove the voltage-dependent Mg^{2+} block. None of the recorded class-1 cells ($n = 11$) responded to NMDA (**Fig. 2d**), but 50% of class-2 neurons did (7/14 cells, **Fig. 2g**). This latter response was fully and reversibly blocked by application of the specific NMDAR antagonist D,L-APV (100 μM) in all tested cells ($n = 5$), which showed an *I*–*V* relationship typical of NMDA current (**Fig. 2g**). We then investigated whether class-1 and class-2 cells express $GABA_A$ receptors. The majority of migrating young neurons recorded from both classes had functional extrasynaptic $GABA_A$ receptors (73% of class 1, $n = 15$; 89% of class 2, $n = 9$). Bath application of a selective agonist of the $GABA_A$ receptor (muscimol) generated a rapidly desensitizing response (**Fig. 2e**). At 25 μM, the mean current induced by muscimol was –56.6 ± 21.7 pA ($n = 8$) and –240.2 ± 100.9 pA ($n = 8$) for class-1 and class-2 cells, respectively, and was always blocked by 20 μM BMI. These results indicate that GC precursors express functional $GABA_A$ receptors and AMPARs very early in their development, while they are still migrating in the RMS. As they arrive and start migrating radially into the GC layer, they begin to express functional NMDARs.

© 2003 Nature Publishing Group http://www.nature.com/natureneuroscience

© 2003 Nature Publishing Group http://www.nature.com/natureneuroscience

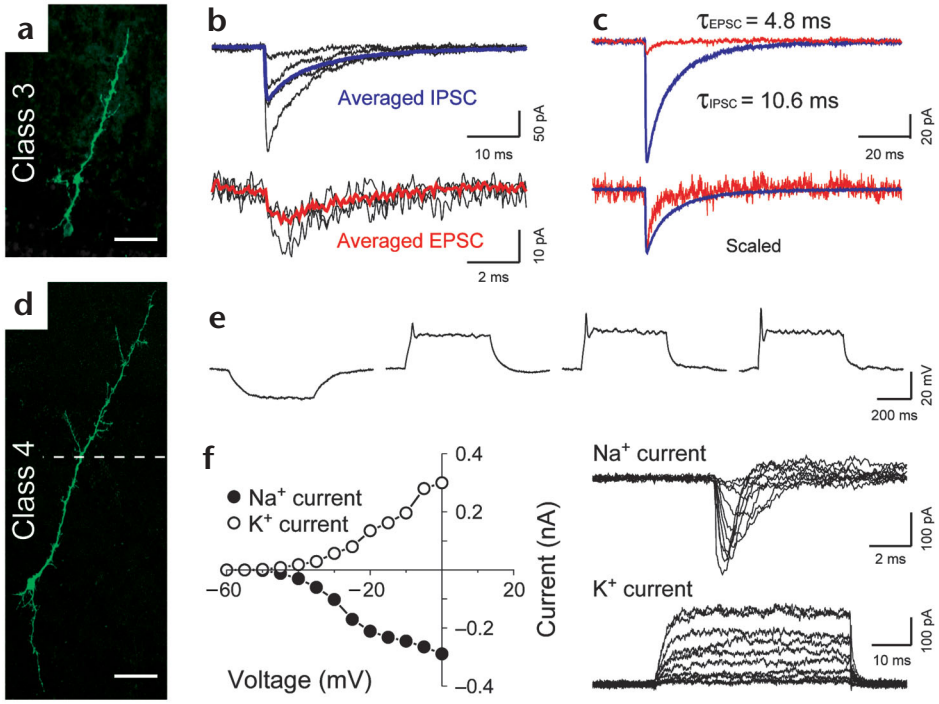

Fig. 3. Functional properties of class-3 and class-4 newborn granule cells. (**a**–**c**) Electrophysiological recordings from a class-3 cell (scale bar in **a**, 25 μm) indicate the presence of spontaneous synaptic events. (**b**) Pharmacological analysis revealed the presence of sIPSCs mediated by $GABA_A$ receptor activation (top, single event in black and average of 35 events in purple) and of sEPSCs mediated by AMPAR activation (bottom, single event in black and average of 20 events in red). (**c**) The averages of the sIPSCs and sEPSCs shown in **b** are superimposed (top) and scaled (bottom). We obtained the τ values from single exponential fittings. (**d**–**f**) Only class-4 neurons (representative photograph shown in **d**; scale bar, 25 μm) showed voltage-gated Na^+ channels that trigger small spikes in current-clamp (**e**). (**f**) The *I*–*V* curves corresponding to the voltage-dependent Na^+ and K^+ currents elicited by increasing depolarizing voltage steps (successive jumps of 5 mV) are presented in the left panel. Individual currents (right) were obtained by subtracting steps before and after 1 μM TTX application for Na^+ currents or before and after 3 mM TEA application for K^+ currents.

Electrophysiological properties of GCs in classes 3 and 4

Whereas cells of classes 1 and 2 showed properties of immature migrating neurons, class-3 (**Fig. 3a**–**c**) and class-4 (**Fig. 3d**–**f**) cells were characterized by the appearance of a small voltage-gated Na^+ current accompanied by synaptic responses. Class-3 cells had apical dendrites that did not reach the mitral cell layer, yet these cells received both spontaneous inhibitory and excitatory postsynaptic currents (sIPSCs and sEPSCs, respectively; **Fig. 3b**,**c** and **7b**–**i**). As application of TTX dramatically reduces the frequency of the spontaneous events[21], it was difficult to analyze the remaining infrequent miniature events. We therefore concentrated our analysis on characterizing only sPSCs.

Under our recording conditions (high Cl^- internal medium to increase the driving force for Cl^- currents), sIPSCs and sEPSCs both triggered inward currents at –60 mV. They could easily be distinguished by differences in kinetics, amplitude (**Figs. 3c** and 7) and pharmacological properties. **Figure 3b** shows examples and the average of unitary sIPSCs mediated by $GABA_A$ receptor activation, since bath application of 20 μM BMI completely abolished them ($n = 26$ from both classes). In the presence of BMI, the remaining synaptic events were AMPA/kainate–mediated EPSCs as revealed by application of 10 μM NBQX ($n = 5$ cells from classes 3 and 4). The presence of sIPSCs was prominent in most class-3 neurons (79% of tested cells, $n = 29$) and virtually all class-4 neurons received GABAergic inputs (97%, $n = 31$). In contrast, only 35% of recorded class-3 neurons ($n = 28$) received sEPSCs, and this proportion increased to 77% for class-4 neurons.

Neurons of classes 3 and 4 could also be distinguished by analyzing the amplitude of the TTX-sensitive voltage-gated Na^+ current. About 38% of class-3 cells ($n = 29$, not shown) expressed small Na^+ current amplitude, not large enough to trigger spikes (0/29 neurons, data not shown). In contrast, 80% of class-4 recorded neurons ($n = 31$) showed a Na^+ current that could occasionally elicit spikes (20% of tested cells; **Figs. 3e** and **5**). In voltage-clamp mode and in the presence of 3 mM TEA, the mean Na^+ current amplitude triggered by a 40-mV depolarization (from –60 mV) was –43.8 ± 3.2 pA for class 3 ($n = 8$) and –296.1 ± 63.3 pA for class 4 ($n = 23$) neurons (**Fig. 3f**). Application of 1 μM TTX to the control medium unmasked the presence of voltage-gated K^+ currents. These results indicate a dramatic maturation step in membrane voltage-gated responses as the newborn cell develops from a class-3 to a class-4 neuron.

Electrophysiological properties of mature GCs

Class-5 cells had the morphology of mature GCs with a fully developed dendritic tree (**Fig. 4a**) containing many spines. To compare class-5 cells with older bulbar interneurons, non-labeled GCs were recorded in the same slices in which GFP^+ class-5 cells were recorded ($n = 9$). We found that the electrophysiological characteristics of class-5 cells were indistinguishable from the surrounding older GCs: the average V_{rest} was –61.2 ± 2.8 mV ($n = 18$) for class-5 neurons and –64.9 ± 2.8 mV ($n = 7$) for older neurons (Mann-Whitney U-test, $P = 0.38$). Both cell types had similar R_m values (class 5, 0.86 ± 0.08 GΩ, $n = 33$; older,

© 2003 Nature Publishing Group http://www.nature.com/natureneuroscience

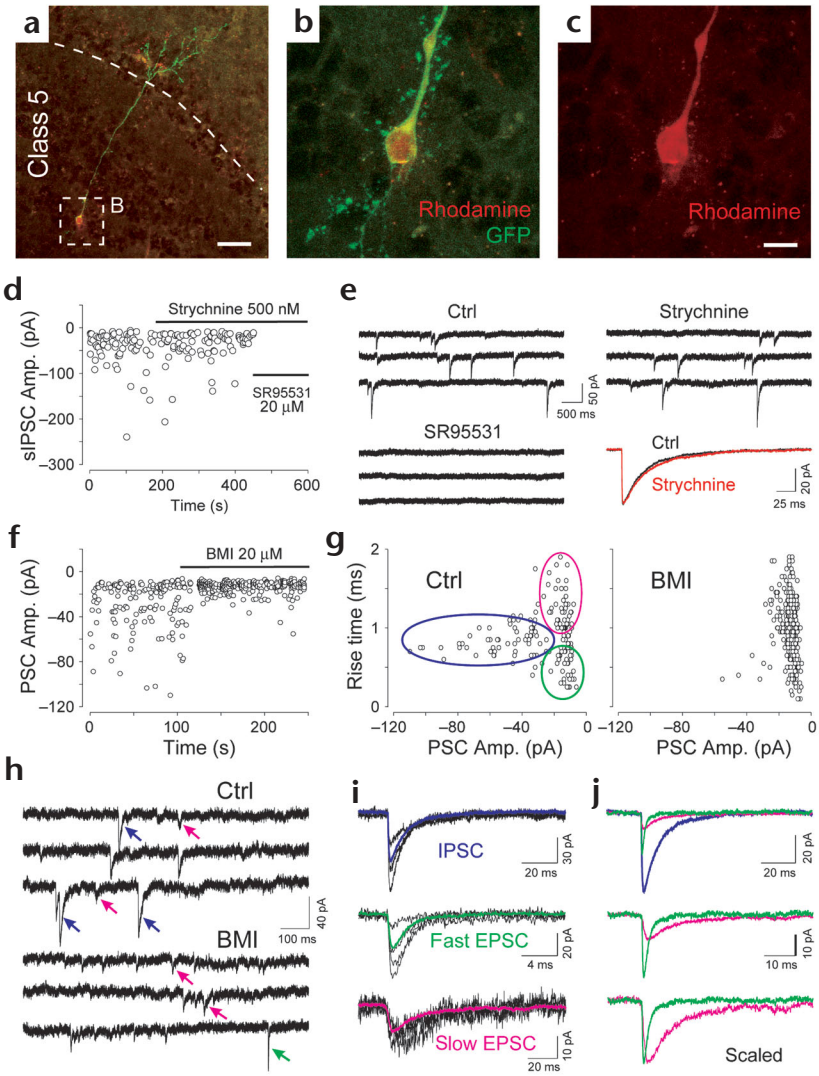

Fig. 4. Functional properties of class-5 newborn granule cells. (**a**–**c**) A class-5 neuron (green) was recorded (**d**, **e**) and filled with dextran-rhodamine (red) before being imaged by confocal microscopy. Higher magnification of the cell body is shown in **b** and **c**. Scale bars, 30 and 6 μm for **a** and **c**, respectively. (**d**, **e**) Pharmacological analysis of sIPSCs observed in the recorded cell presented in (**a**–**c**). The time course of drug applications is indicated by horizontal bars in **d**. The neuron was recorded in the presence of 10 μM NBQX and 100 μM D,L-APV. Strychnine affected neither the frequency nor the amplitude of the inhibitory events (compare representative traces shown at the top in **e**). The decay time course of the average IPSC was not affected by strychnine (**e**, bottom-right traces; average of 48 events under both conditions, τ_{ctrl} = 32 ms and $\tau_{strychnine}$ = 36 ms). Subsequent application of the specific $GABA_A$ receptor antagonist SR95531 abolished all sIPSCs (**d** and **e**). (**f**–**j**) Spontaneous PSCs were observed during the recording of another class-5 neuron. (**f**) Pharmacological analysis revealed the presence of $GABA_A$ receptor–mediated sIPSCs, as bath application of BMI antagonized a population of large synaptic events, leaving sEPSCs intact. (**g**) Graphs showing the relationship between sPSC rise time versus amplitude in control medium (left) and after BMI application (right). Colored ellipses correspond to three populations of different amplitude and rise time. The blue ellipse delimits the BMI-sensitive IPSCs, and the two remaining populations showed EPSCs with either a fast (green) or a slow (red) rise time. (**h**) Sample recordings of the traces shown in **i**. Arrows indicate synaptic events (color code same as in **g**). (**i**) Unitary IPSCs, fast EPSCs and slow EPSCs (top, middle and bottom traces, respectively) are superimposed with the corresponding trace averaged from 35, 18 and 58 events, respectively. (**j**) The average PSCs shown in **i** are superimposed (top and middle traces) and scaled (bottom traces). The decay time was fitted with a single exponential: τ_{IPSC} = 10.2 ms, $\tau_{fastEPSC}$ = 2.1 ms and $\tau_{slowEPSC}$ = 9.2 ms. All neurons were held at –60 mV.

0.80 ± 0.16 GΩ, $n = 8$; $P = 0.74$) and C_m values (15.9 ± 0.8 pF, $n = 33$ versus 13.8 ± 1.1 pF, $n = 8$; $P = 0.37$).

Furthermore, recordings from class-5 neurons ($n = 34$) revealed fast voltage-gated Na^+ currents that triggered spikes in the majority of recorded cells (88%). In bath medium containing NBQX (10 μM) and D,L-APV (100 μM), all class-5 neurons showed sIPSCs with a mean frequency of 0.66 ± 0.15 Hz ($n = 34$, **Fig. 4d–g**) not different from mature GCs (0.49 ± 0.09 Hz, $n = 7$, Kolmogorov-Smirnov test, $P > 0.05$). These IPSCs showed a slow decay (mean 16.8 ± 7.1 ms, $n = 34$) similar to that of mature GCs (17.7 ± 2.6 ms, $n = 7$, $P > 0.05$). Both decay time and frequency were highly variable (**Fig. 7c**). Bath application of TTX did not alter the kinetics ($n = 5$, Wilcoxon pairs test, $P > 0.05$), showing that $GABA_A$-mediated events did not result from a difference between spontaneous and miniature synaptic events. Addition of 500 nM strychnine, a glycine receptor antagonist, did not affect the frequency (0.43 ± 0.05 Hz before and

© 2003 Nature Publishing Group http://www.nature.com/natureneuroscience

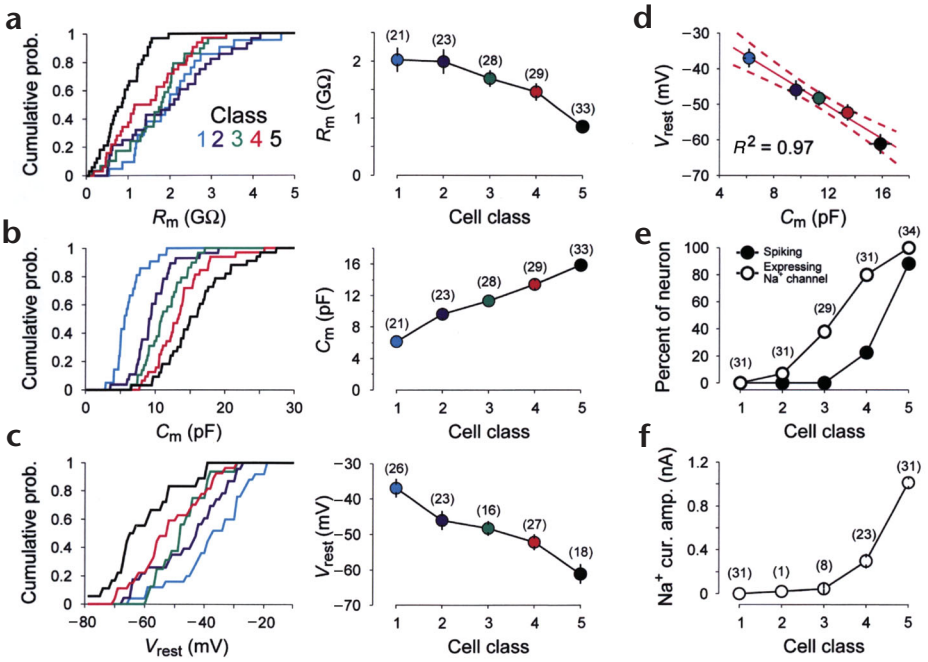

Fig. 5. Summary graphs of changes in intrinsic membrane properties during neuronal maturation. (**a**–**c**) Input membrane resistance (R_m, **a**), cell membrane capacitance (C_m, **b**) and resting membrane potential (V_{rest}, **c**) are presented either as cumulative plots (left graphs; each colored line represents data collected from one class of cells) or as mean values (right graphs; the number of tested cells is indicated in parenthesis). (**d**) Linear correlation (plain line) between V_{rest} and C_m (R^2, square regression index). Dotted lines indicate the 5% confidence band linear regression. (**e**) Percentage of recorded GFP^+ cells in each class that displayed spikes (black dots) or voltage-gated Na^+ currents (white dots); the number of cells is indicated in parenthesis. (**f**) Mean amplitude of the Na^+ current triggered by voltage-step of +40 mV (the number of cells is indicated in parentheses).

0.41 ± 0.06 Hz during strychnine treatment, $n = 4$, **Fig. 4d**), amplitude (–34.5 ± 6.9 pA before and –34.7 ± 6.9 pA during strychnine treatment; **Fig. 4e**) or decay time (25.5 ± 2.7 ms before and 26.9 ± 3.4 ms during strychnine treatment; **Fig. 4e**). Thus, heterogeneity of time decays did not result from glycinergic receptor participation, as also shown by the use of specific $GABA_A$ receptor antagonists SR95531 and BMI ($n = 28$; **Fig. 4d** and **e**).

In standard medium, excitatory and inhibitory synaptic events were distinguished by their respective amplitudes and kinetics (colored ellipses in **Fig. 4g**). $GABA_A$-mediated events were characterized by large amplitudes (**Fig. 4f**) and fast rise times (**Fig. 4g**, blue ellipse). In the presence of BMI, the frequency of excitatory synaptic events increased from 3.45 ± 0.7 Hz to 9.46 ± 1.38 Hz ($n = 19$, Wilcoxon pairs test, $P < 0.0005$). These sEPSCs, which were totally blocked by NBQX (10 μM, $n = 8$), could further be subdivided into two populations (**Fig. 4g**) according to their fast (mean 0.5 ms, green ellipse) or slow (mean 1.5 ms, red ellipse) rise time. The traces in **Fig. 4h** illustrate the different synaptic activities (with the same color code as in **Fig. 4g**) and reveal that sEPSCs can be further distinguished by their decay times (**Fig. 4i** and **j**). We infer that class-5 neurons receive two distinct glutamatergic inputs with different kinetics.

Intrinsic membrane properties during maturation

All GFP^+ neurons recorded in the RMS (class-1 cells) were found to be silent, even during prolonged recordings, with relatively high R_m, low C_m and depolarized V_{rest} values (**Fig. 5**). Through the different maturation stages, a striking correlation was found between the passive membrane properties and the neuronal class. Maturation of newborn neurons was accompanied by a progressive decrease in R_m (**Fig. 5a**). In contrast, C_m, a parameter proportional to the cell surface area (thus to dendritic length), increased in parallel with the morphological maturation (**Fig. 5b**). Concomitantly, a gradual hyperpolarization of V_{rest} (**Fig. 5c**) was observed as the cells grew, indicating progressive changes in internal ionic concentrations and/or membrane conductances (see **Supplementary Table 1** online). This progressive hyperpolarization was also correlated with the degree of dendritic maturation as shown by the strong correlation between V_{rest} and C_m (**Fig. 5d**). Thus, intrinsic membrane properties could predict the state of maturation of newborn neurons: high R_m cells tended to have shorter dendritic arbors and depolarized V_{rest}. Associated with the hyperpolarizing V_{rest}, we found that the expression of Na^+ currents increased with neuronal maturation (**Fig. 5e**). Surprisingly, only the most mature neurons (starting with a minority of class-4 cells) were able to fire action potentials. The lack of excitability of newborn neurons from class 1 to class 4 seemed to result from small Na^+ current amplitudes (**Fig. 5f**).

To further investigate this late appearance of action potentials, the expression of the α subunit of voltage-gated Na^+ channels was studied at different stages of maturation of the newly formed OB interneurons (**Fig. 6**). Cells were probed by immunocytochemistry using an anti-α antibody that recognizes all of the α isoforms of the Na^+ channel (panNav; Methods). We found that neurons of class 1 and 2 did not express Na^+ channel (data not shown). In neurons of classes 3 and 4 (**Fig. 6a–j**), the α subunit was present in the cytoplasm around the nuclei (**Fig. 6e** and **f**). In the more mature class-4 (with a more complex dendritic arborization) and all class-5 neurons, staining of the α subunit of the Na^+ channel was more consistent (**Fig. 6g–j**). These observations suggest that Na^+ channels begin to be expressed

© 2003 Nature Publishing Group http://www.nature.com/natureneuroscience

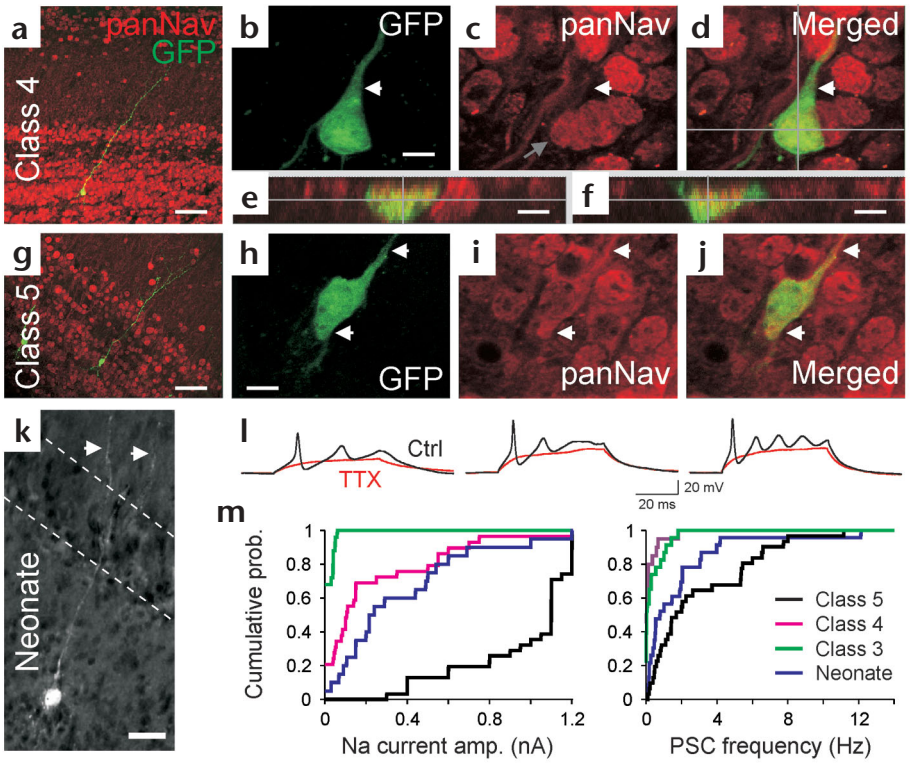

Fig. 6. Delayed maturation of excitability is a feature of adult neurogenesis. (**a**–**f**) A typical class-4 cell that does not display voltage-gated Na^+ channel (panNav) staining at the plasma membrane. The GFP^+ cell has a dendrite reaching the EPL but was moderately developed (**a**). (**b**–**d**) The somatic plasma membrane (white arrow) is not labeled with panNav, though a perinuclear staining is observed in the confocal *xy* projection image (gray arrow, **c**). This is confirmed in the *xz* (**e**) and *yz* (**f**) plane single scan images obtained through the cell body (same neuron as in **c**). (**g**–**j**) A class-5 cell with a branched dendritic tuft located in the EPL is stained with panNav at the membrane surface. The white arrows point out the somatic and proximal dendritic membrane staining. (**k**–**m**) Electro-physiological recordings of neonate (P2–P4) olfactory bulb GCs. (**k**) Rhodamine staining of a recorded cell. The dendrite crosses the MCL (between dotted lines) and bifurcates (white arrows) in the EPL. Although the cell does not receive synaptic events (not shown), it emits TTX-sensitive spikes upon three increasing depolarization steps (**l**). (**m**) Na^+ current amplitude (left) and PSC frequency (right) values obtained from the neonate and the adult neuronal classes are presented as cumulative plots.

soon after cells complete migration and can reliably be detected only after cells have matured to class 4–5.

Delayed spiking activity in adult-generated interneurons

These results suggest that new neurons produced in the adult brain are non-spiking during most of their maturation, probably due to a delay in targeting Na^+ channels to the plasma membrane. To test this idea and to investigate whether a similar phenomenon was taking place in new bulbar interneurons that mature in the early postnatal brain when olfactory circuits are not yet mature, we studied GCs by patch-clamp recordings in P2–P4 animals (**Fig. 6k–m**). Although the dendritic arborization of GCs was not as complex as for class-5 cells in the adult, intrinsic electrophysiological parameters were similar to those of class-5 neurons. Neonate GCs had a V_{rest} of -61 ± 2 mV ($n = 20$), not different from class-5 neurons (M-W test, $P > 0.05$). About 95% expressed TTX-sensitive Na^+ current ($n = 20$), and more than 70% showed action potential firing. A comparison of the distribution of Na^+ current amplitudes recorded among neonate- and adult-generated cells is shown in **Fig. 6m**. The neonate GC population displayed greater Na^+ currents (-378 ± 72 pA, $n = 20$) than both class-3 (-14 ± 4.3 pA, $n = 25$; M-W test, $P < 10^{-7}$) and class-4 (-234.8 ± 54.9 pA, $n = 29$; $P < 0.05$) adult born GCs. Although neonate neurons showed a rather mature excitability, most of these cells remained synaptically silent. Only very few cells received synaptic events with a frequency lower than that detected in class-3 cells (neonate, 0.19 ± 0.1 Hz, $n = 20$; class 3, 0.33 ± 0.1 Hz, $n = 23$; **Fig. 6m**). For example, the recorded neonate GC shown in **Fig. 6k** fired action potentials (**Fig. 6l**) but did not received synaptic inputs. This was never seen in adult-generated GCs where synaptic inputs were present from early stages of maturation (class 3), yet spiking activity did not appear until cells were nearly mature. For example, class-4 neurons received ten times more synaptic events than neonate cells but less than 20% showed spiking activity. In summary, an early onset of synaptic inputs impinging on non-spiking neurons is apparently unique to neurons born in adults.

Synaptic activities during neuronal maturation

Our analysis of the developmental appearance of various transmitter receptors at different maturation stages indicated that extrasynaptic $GABA_A$ receptors were the earliest to appear in newly generated neurons (**Fig. 7a**). Class-1 neurons predominantly expressed extrasynaptic $GABA_A$ receptors (73%, $n = 15$ neurons), whereas functional AMPARs were only present in 28% of tested cells (**Supplementary Table 1**). Furthermore, we never found cells with AMPA currents in the absence of $GABA_A$ responses. Interestingly, extrasynaptic NMDARs were not detected on class-1 cells ($n = 11$, **Fig. 7a**). This data supports the idea that neurons with both $GABA_A$ and glutamate receptors were more developed than those with $GABA_A$ receptors alone. When

© 2003 Nature Publishing Group http://www.nature.com/natureneuroscience

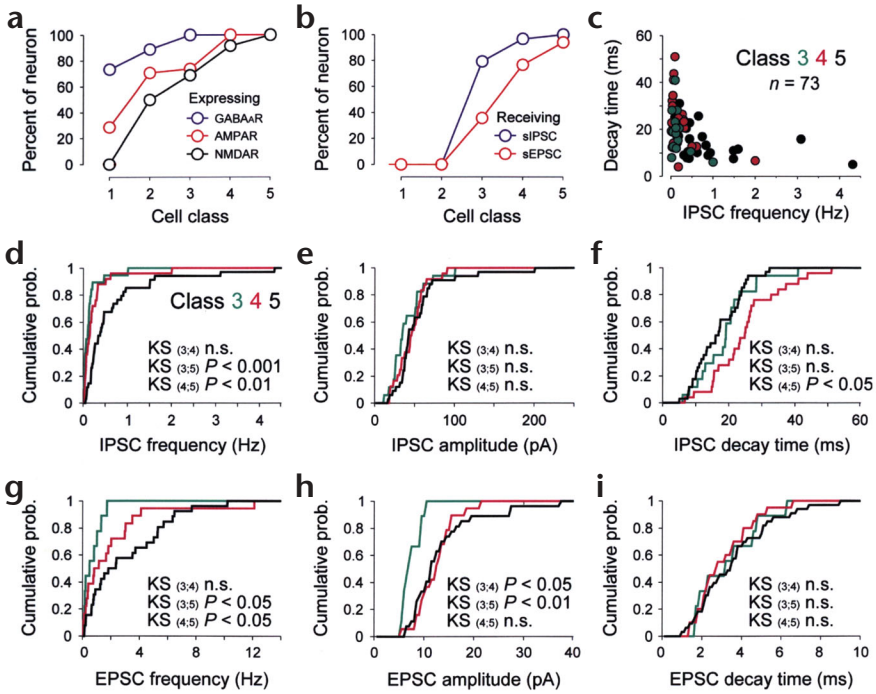

Fig. 7. Changes in synaptic activity during neuronal maturation. (**a**) Percentage of GFP$^+$ cells in each class expressing functional $GABA_A$ receptors, AMPARs and NMDARs (blue, red and black lines, respectively) and (**b**) receiving inhibitory (blue curve) and excitatory (red curve) postsynaptic currents (see **Supplementary Table 1** for the number of tested cells). (**c**) Graph showing the relationship between the IPSC frequency and its average decay time. Each dot represents an individual recorded cell; color code used in **c**–**i** indicates the class to which the cell belongs (green, red and black for class 3, 4 and 5 respectively). (**d**–**f**) IPSC frequency (**d**), average amplitude (**e**) and average decay time (**f**) values obtained from the different neuronal classes are presented as cumulative plots (statistical significance is given by the K-S test; numbers in parentheses indicate the compared classes). (**g**–**i**) Summary graphs of EPSC frequency (**g**), amplitude (**h**) and decay time (**i**).

comparing glutamate-responding neurons, those expressing NMDARs were more mature than those that showed only AMPA responses (**Supplementary Table 1**).

Spontaneous synaptic events were recorded from class-3 and more mature neurons (**Figs. 6m** and **7b**). Consistent with the observed sequence of maturation of extrasynaptic receptor-mediated responses, inhibitory synapses appeared before excitatory events. About 80% of class-3 cells ($n = 29$) showed sIPSCs, whereas only 36% ($n = 28$) showed sEPSCs, and none of them received sEPSCs without sIPSCs. The number of neurons receiving synaptic inputs increased with maturation (**Fig. 7b**). Notably, sIPSC frequency increased sharply from class 4 to 5 cells (**Fig. 7d**), whereas changes in sEPSCs were more gradual (**Fig. 7g**). This increase was unexpected given that class 4 and 5 cells differ in their dendritic complexity within the EPL, whereas $GABA_A$ inputs occur only at the somato-dendritic compartment located in the GC layer[22] (**Supplementary Fig. 1**).

Whereas the amplitude of sIPSCs remained constant as new neurons matured (**Fig. 7e**), the amplitude of sEPSCs increased significantly with cell maturation (**Fig. 7h**). In contrast, EPSC decay times were similar throughout maturation (**Fig. 7i**), and IPSC decay times significantly changed from class 4 to 5 neurons (**Fig. 7f**). Decay times were highly variable, ranging from 5 to 51 ms ($n = 73$), even when the recorded cells belonged to the same developmental class (**Fig. 7c** and **f**). Having discarded differences in synaptic input location (**Supplementary Fig. 1**), we searched

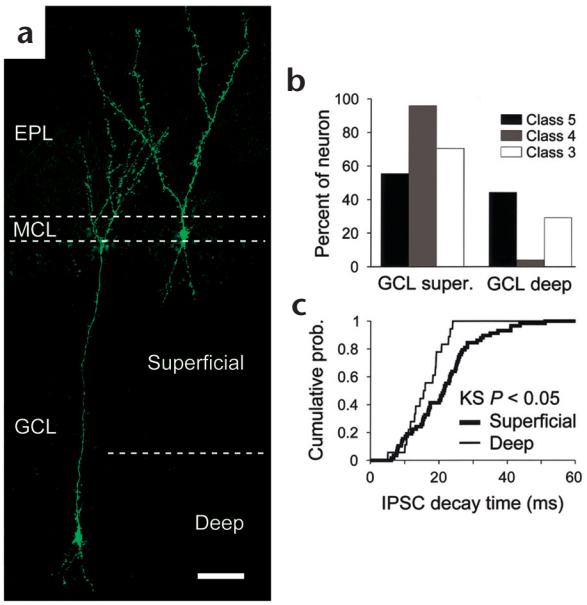

Fig. 8. Two populations of newborn granule cells were distinguished according to their location in the GC layer. (**a**) Photomicrograph showing two mature newborn GCs located in the superficial and deep regions of the GC layer; the dotted line divides the layer into an upper and lower part of the GC layer (scale bar, 45 μm). EPL, external plexiform layer; MCL, mitral cell layer. (**b**) Summary graph showing within each class the percentage of the recorded newborn GCs located in the upper and lower part of the GC layer. (**c**) Cumulative plot comparing the IPSC decay time values measured from GCs recorded either in the superficial part (thick line) or the deep part of the GC layer (thin line).

© 2003 Nature Publishing Group http://www.nature.com/natureneuroscience

for possible sources of variability. In agreement with previous reports[12], we noticed that class-5 neurons showed different dendritic morphologies depending on the location of their soma (**Fig. 8a**). We thus distinguished new neurons whose cell body resides close to the mitral cell layer from deeper GCs with a cell body closer to the core of the OB (**Fig. 8a** and **b**). Using this criterion, IPSC decay times were consistently slower in superficial GCs compared to deeper GCs (superficial, 21.3 ± 1.3 ms, $n = 55$; deeper, 15.9 ± 1.2 ms, $n = 18$; K-S test, $P < 0.05$, **Fig. 8c**). This difference could, in theory, reflect distortion by electronic filtering, but this was ruled out because superficial and deep GCs had similar IPSC rise times (superficial, 0.79 ± 0.04 ms, $n = 55$; deeper, 0.85 ± 0.09 ms, $n = 180$; $P > 0.05$) and amplitudes (superficial, –47 ± 3 pA, $n = 55$; deeper, –49.6 ± 9.3 pA, $n = 18$; $P > 0.05$, data not shown). Thus, the two distinct time courses of inhibitory events may rather reflect differences in the composition of the postsynaptic $GABA_A$ receptor, the rate of clearance from the synaptic cleft, the time-course of GABA release and/or the occurrence of GABA overlap from neighboring release sites.

Discussion

Previous studies based on morphology[5,7] or neuronal markers[8–10] suggest that adult SVZ stem cells give rise to new neurons that integrate into the adult OB, but here we have identified and characterized these neurons using physiological criteria. As first shown in adult canaries[11] and then in adult mammalian hippocampus[17,18], electrophysiological recordings provide conclusive evidence that newborn cells correspond to neurons. Here we show that newly formed GCs fire action potentials spontaneously and receive synaptic contacts, suggesting that they are functionally integrated into OB circuitry. Previous *in vitro* studies suggest that neurons derived from adult progenitor cells possess immature properties[20,23,24]. Our results suggest that newly formed SVZ cells become functionally mature interneurons with properties similar, if not identical, to older GCs. In addition, we describe the functional properties of new neurons, not only once they express neuronal markers, but also through the different stages of their maturation.

How immature neurons differentiate during development has been a subject of many studies, but little is known about the process governing neuronal maturation in the adult brain. Unlike in the developing brain where neurogenesis usually precedes the maturation of neural circuits, in the adult OB, new neurons have to integrate into a preexisting neuronal network. Our data show that some of the functional properties of immature neurons in the adult brain are similar to those described for the developing brain, but others are unique. This suggests that integration of new neurons into adult circuits may be subjected to some constraints.

Properties of migrating neurons in the adult brain

Tangentially migrating (class 1) cells in the RMS first expressed extrasynaptic $GABA_A$ receptors and then AMPARs. Within many brain regions, GluR2-containing AMPARs are developmentally regulated, with low GluR2 being observed at early developmental stages. This was not the case for neurons born in the adult SVZ. Indeed, immature class-1 cells express AMPARs containing GluR2 before NMDARs appear in class-2 cells. Again, this differs from the developing mammalian brain where, most often, NMDARs are first detected and functional AMPAR recruitment is induced by NMDAR activation[25]. We found that adult-generated GCs receive synaptic inputs shortly after completing their radial migration as they began developing their dendritic arbor. In these cells, GABAergic synaptic events appear before glutamatergic ones. In sharp contrast with prenatal development, we found that maturing neurons receive both $GABA_A$-mediated events and excitatory synaptic inputs before being able to generate action potentials.

Little is known about the electrophysiological properties of tangentially migrating neuroblasts. It will be interesting to determine the function of GABA receptors in tangentially migrating cells and whether activity of these receptors is required for subsequent maturation, including the appearance of voltage-gated channels. The signals that determine when cells separate from the chains and initiate radial migration remain to be identified. We found that tangentially and radially migrating cells differ in their expression of functional NMDARs. These receptors may appear in radially migrating neurons as a detector of local levels of neuronal activity and may hasten the maturation and differentiation of young cells through Ca^{2+} entry as suggested during development[26]. Such a function would be consistent with our observation that radially migrating GCs have a sufficiently depolarized V_{rest} to remove the Mg^{2+} block from NMDARs.

Intrinsic membrane properties of adult-generated cells

The maturation of passive membrane properties that we describe is similar to that reported during development[27,28]. We found that during the maturation of new GCs, R_m decreases as the density of ionic channels increases. It may also be possible that the development of gap junctions could contribute to the decrease in R_m. The high R_m values found in cells recorded in the RMS strongly suggest that gap junctions are absent at this early stage of maturation. This observation is also consistent with the absence of Na^+ channels and with the low density of K^+ channels found in class-1 cells.

Since V_{rest} is determined primarily by non-gated K^+, Cl^- and Na^+ channels[29], the progressive hyperpolarization we observed during maturation of the new neurons may reflect an increase in channel densities and/or alterations in the internal concentration for the corresponding ions. We found that SVZ precursors recorded in the RMS extension had a V_{rest} of –37 mV, an incipient K^+ current and remained unable to generate spikes. The lack of firing activity was also observed in cultured SVZ precursors[20]. Surprisingly, we found that spiking was the latest property acquired by newborn interneurons (see below).

Synaptic activities in adult-generated neurons

In many neuronal systems, activity-dependent refinement and remodeling of initially coarse patterns of synaptic connections is required for the development of fully functional networks. However, it is not yet clear whether the same principle applies to neurons that integrate into already-functional circuits in the adult brain. It was of particular interest to determine when and what kinds of synapses are first established onto the newly formed neurons. We found that synaptic connections first appear in class-3 neurons, shortly after the precursors have stopped their radial migration and while they are still growing dendrites. New neurons in adult OB first receive GABAergic synapses and then glutamatergic ones. This is similar to what has recently been described in the neonate hippocampus[30,31], but the transition appears to occur more rapidly in the adult OB. Whereas class-2 cells never display synaptic events, more than 80% of class-3 cells receive GABAergic inputs and about 35% exhibit glutamatergic events. The initial glutamatergic contacts onto newborn neurons may arise from mitral cell axonal collaterals or from centrifugal fibers[12] as class 3 cells do

© 2003 Nature Publishing Group http://www.nature.com/natureneuroscience

not yet have dendrites reaching the EPL. A second population of glutamatergic inputs appears later when the GC tuft is formed (class 5). The progressive increase in EPSC frequency shown in **Fig. 7g** and the appearance of larger EPSCs (**Fig. 7h**) for class 5 cells may reflect the formation of the reciprocal dendro-dendritic synapses with mitral cell lateral dendrites. Consistently, the increase in number and length of newborn GC dendrites reaching the EPL coincides with the appearance of a second wave of excitatory inputs. This suggests that the dendritic length of newborn GCs may have to reach a certain size before additional glutamatergic synapses can be established as demonstrated for hippocampal pyramidal neurons[30,31]. Conversely, the formation of the initial glutamatergic synapses could trigger dendritic growth[32].

Early onset of GABAergic synapses on newborn neurons

In many immature brain regions, the primary inhibitory transmitter in the mature brain, GABA, first provides excitatory drive in the embryonic or neonatal brain[24,33–35]. The shift from the depolarizing to the hyperpolarizing action of GABA is mediated by changes in $[Cl^-]_i$ that generally occurs at the end of the first postnatal week[33–35]. The depolarizing effects of GABAergic synapses during development are considered a milestone of developing networks and have been confirmed in many species and structures[34]. In our study, GABA mediated the first extrasynaptic responses seen in migrating cells. The early expression of $GABA_A$ receptors agrees with a recent report showing that cultured SVZ precursor cells express only $GABA_A$ receptors[24]. In our preliminary experiments using the gramicidin perforated patch-clamp technique, E_{Cl} was found to be -21.2 ± 1.4 mV in class-1 cells ($n = 3$), indicating that activation of GABA receptors depolarizes tangentially migrating SVZ progenitor cells from their mean V_{rest} of –37 mV. This observation, combined with a recent finding that a subset of adult SVZ precursor cells contains GABA[36], suggests that GABA receptors may control the cell migration within the RMS.

GABA enhances neurite outgrowth, increases synapse formation, modulates cell migration and promotes the developmental switch of neuronal GABAergic responses from excitation to inhibition[33–35]. Similarly, acquisition of early $GABA_A$ receptors in class-1 cells may be critical for their maturation. The question of how $GABA_A$ receptors expressed by class-1 cells are activated remains unanswered because migrating cells do not form synapses, as indicated by electron microscopy[37] and by the lack of spontaneous synaptic currents (present results). One possibility is that endogenous extracellular GABA could activate $GABA_A$ receptors by a non-synaptic mechanism. It is also possible that migrating neuroblasts could themselves release GABA to activate neighboring migrating cells in a paracrine manner.

It would be interesting to determine precisely when the E_{Cl} switch occurs during neuronal maturation. Based on V_{rest} values shown in **Fig. 5c**, it is difficult to predict whether class-3 neurons receive excitatory or inhibitory $GABA_A$ synaptic inputs. Unlike developing neurons in other systems, young GCs formed in the adult OB acquire the ability to generate action potentials only very late in their maturation. Thus, even if GABA is excitatory in stage-3 neurons, it does not trigger cell spiking, as newborn neurons quietly integrated into the bulbar circuits, became connected and only then began firing spikes. In the developing brain, in contrast, excitatory GABA participates in network synchronous activities[34,38]. The adult mechanism may protect already-functional circuits from uncontrolled neurotransmitter release and network disruptions.

Contribution of adult-generated interneurons in the OB

Previous observations in the hippocampus suggest that new neurons bring unique properties into adult circuits. The form of plasticity seen in young GCs in the adult dentate gyrus is different from that observed in older GCs[39]. New neurons also respond preferentially to the modulation mediated by stress hormones[40], to spatial learning[41] and to exercise[42]. Similarly, increasing the number of newborn interneurons in the OB improves olfactory memory[43], whereas decreasing it alters odor discrimination[13,14]. The multiple stages in the maturation of newborn neurons that we have described here may serve as a substrate for plasticity. They could provide the OB with a large repository of plastic cells to better respond to changes in the environment. Interestingly, one of the forms of plasticity may reside in the type of neurotransmitter released by newly formed cells. We have recently reported that some GCs, previously considered as a homogeneous population of GABAergic neurons, release glutamate onto mitral cell lateral dendrites[44]. Similarly, it has recently been shown that glutamatergic GCs of the dentate gyrus actually release both glutamate and GABA[45,46]. It is possible that new bulbar GCs could use both neurotransmitter systems, or release glutamate only transiently, at early stages of their maturation.

The sense of smell has had a central role mammalian evolution. Odor representation is dynamic and highly complex, perhaps requiring a unique mechanism of plasticity. Neurogenesis, migration and maturation of new neurons in the OB are likely part of this adaptive mechanism. It takes about two weeks for a new SVZ neuron to become part of the existing circuit in the OB, and during this time, it undergoes a series of unique maturational stages. Each of these functional stages could contribute to plasticity. The presence of young neurons at different stages of differentiation in the active OB may allow for adjustments in the way these cells become integrated. As it takes time for new neurons to extend neurites and become synaptically integrated, bulbar neurogenesis may contribute to long-term adjustment of the OB circuitry rather than to acute plastic changes. However, other mechanisms may also take advantage of new neurons. More than half of the new interneurons in the OB die within a month after they reach their mature state[10]. The present results confirm that during this period of fast cell death, newborn GCs are synaptically connected. Selective elimination of neurons may allow for rapid modification of circuitry. The ability to mold how new neurons become integrated, and to continually eliminate older cells without depleting the neuronal population, may bring into neuronal networks a degree of circuit adaptation unmatched by synaptic plasticity alone.

METHODS

Retroviral vector construction. A replication-incompetent retroviral vector encoding eGFP (Clontech Laboratories, Palo Alto, California) was used to label cells. For a better visualization during electrophysiological recordings, eGFP was tagged with a GAP-43 sequence to target the GFP to the cell membrane. The construction, purification and storage of retroviral vectors were done as previously described[15]. Stock concentration was ~10^9 infectious particles per ml. In some experiments, a viral construct in which eGFP was fused to the human histone H2B gene was also used to target the eGFP to the nucleus[47]. Neurons infected by either construct showed similar physiological properties. Thus, GFP targeting to the plasma membrane does not alter the electrophysiological properties, and it was preferentially used because it offers a more precise visualization of plasma membranes.

Animals and stereotaxic injections. Injections of retroviral particles were done stereotaxically on more than 80 male mice of about 10 weeks old (C57BL/6J; Iffa Credo, L'Arbresle, France). Animals were anesthetized

© 2003 Nature Publishing Group http://www.nature.com/natureneuroscience

by an intraperitoneal injection of pentobarbital (25 mg per kg of body weight). About 200 nl of retroviral stock solution was injected at two sites for each hemisphere (coordinates relative to Bregma: A, 1 mm; L, ±1 mm; D, 2.2 mm and A, 0 mm; L, ±1.4 mm; D, 1.6 mm). The bevel and small diameter of the pipette tip results in very little brain damage, but we cannot exclude the possibility that proliferation was altered by stereotaxic injections. This is not problematic for the present work, as we did not quantitatively analyze neurogenesis, and our recordings of newborn neurons were performed far from the injection sites. All experimental procedures were done in accordance with the Society for Neuroscience and European Union guidelines and were approved by our respective institutional animal care and use committees.

Immunohistochemistry. At 50 days after viral infection, 12 mice were given an overdose of sodium pentobarbital (100 mg/kg; Sanofi, France) and perfused transcardially with 50 ml of saline containing heparin (5×10^3 U/ml) at 37 °C followed by 200 ml of 4% paraformaldehyde (PFA) in 0.1 M phosphate buffer at 4 °C (PBS, pH 7.3). The brains were then dissected out and fixed overnight in 4% PFA. They were embedded in 4% agar and 40 μm-thick horizontal slices were prepared with a vibratome (Leica) and collected in PBS (0.1 M). Slices were preincubated in 3% normal horse serum, 3% BSA and 0.1% Triton X-100 in PBS for 1 h. Primary rabbit polyclonal anti-GAD67 (1:1,000, Chemicon), anti-sodium channel (SP19, 1:400, Sigma) and mouse monoclonal anti-NeuN (1:200, Chemicon) antibodies, diluted in PBS containing 0.05% Triton X-100, were applied overnight. Secondary anti-rabbit IgG and anti-mouse Alexa-568 antibodies (1:1,000, Molecular Probes), diluted in PBS, were applied for 3 h. Sections were washed in PBS, covered with Vectashield (Vector Laboratories, Burlingame, California) and fluorescent images were obtained with a Leica TCS SP2 confocal microscope equipped with Ar laser 488 and HeNe laser 543.

Electrophysiological recordings. Adult recordings were performed as previously described[21] on horizontal OB slices (300 μm). GFP^+ cells were identified and recorded under video-assisted differential interference contrast with an upright Zeiss Axioskop microscope. The morphology of recorded cells was observed using 0.4% dextran-rhodamine (Sigma, St. Louis, Missouri) in the internal pipette solution. Only cells expressing GFP and subsequently labeled with rhodamine were taken into account in this study.

Neonate (P2–P4) C57/Bl6J mice were killed by cervical dislocation after Isoflurane anesthesia (Belamont, Neuilly-sur-Seine, France). The brain was dissected out and rapidly incubated in cold oxygenated (5% CO_2 and 95% O_2) ACSF. Horizontal slices (200 or 300 μm) were obtained from brains embedded in 4% agar with a vibrating microtome (VT-1000, Leica, Argenteuil, France) and kept in oxygenated ACSF at 32 °C for about 30 min. Subsequently, the slices were stored at room temperature (20–22 °C) for 4–6 h. Individual slices were then transferred to a submerged-slice recording chamber where they were superfused with oxygenated ACSF at a rate of 2–3 ml/min.

During patch-clamp recordings, cells were bathed with a Ringer's solution containing 124 mM NaCl, 3 mM KCl, 2.4 mM $CaCl_2$, 1.3 mM $MgSO_4$, 25 mM $NaHCO_3$, 1.25 mM NaH_2PO_4 and 10 mM D-glucose; pH 7.3 when saturated with 95% O_2 and 5% CO_2 (310 mOsm). The internal pipette milieu contained 135 mM KCl, 8 mM NaCl, 0.2 mM K-EGTA, 10 mM Na-HEPES, 10 mM D-glucose, 0.3 mM GTP, 2 mM Mg-ATP, 0.2 mM AMPc and 0.1 mM spermine; pH 7.3 (280 mOsm). V_{rest} was estimated just after breaking the membrane in the cell-attach mode. NMDA, muscimol and D-serine were obtained from Tocris (Ellisville, Missouri); all other drugs and salts were purchased from Sigma (Saint Quentin Fallavier, France).

Note: Supplementary information is available on the Nature Neuroscience website.

Acknowledgments

This work was supported by the Pasteur Institute, the Annette Gruner-Schlumberger Foundation, the CNRS, the Fondation pour la Recherche Médicale, a grant from the French Ministry of Research and Education (ACI Biologie du Développement et Physiologie Intégrative 2000) and by a National Institutes of Health grant HD32116. We thank E. Perret and M.M. Gabellec for technical help with the confocal microscope and immunocytochemistry, respectively. We also thank A. Saghatelyan, M. Davenne and I. Manns for critical reading of the manuscript.

Competing interests statement

The authors declare that they have no competing financial interests.

RECEIVED 6 FEBRUARY; ACCEPTED 11 MARCH 2003

1. Alvarez-Buylla, A. & Garcia-Verdugo, J.M. Neurogenesis in adult subventricular zone. *J. Neurosci.* **22**, 629–634 (2002).
2. Gage, F.H. Neurogenesis in the adult brain. *J. Neurosci.* **22**, 612–613 (2002).
3. Nottebohm, F. Why are some neurons replaced in adult brain? *J. Neurosci.* **22**, 624–628 (2002).
4. Wichterle, H., Turnbull, D.H., Nery, S., Fishell, G. & Alvarez-Buylla, A. *In utero* fate mapping reveals distinct migratory pathways and fates of neurons born in the mammalian basal forebrain. *Development* **128**, 3759–3771 (2001).
5. Luskin, M.B. Restricted proliferation and migration of postnatally generated neurons derived from the forebrain subventricular zone. *Neuron* **11**, 173–189 (1993).
6. Lois. C. & Alvarez-Buylla, A. Long-distance neuronal migration in the adult mammalian brain. *Science* **264**, 1145–1148 (1994).
7. Kishi K. Golgi studies on the development of granule cells of the rat olfactory bulb with reference to migration in the subependymal layer. *J. Comp. Neurol.* **258**, 112–124 (1987).
8. De Marchis, S., Fasolo, A., Shipley, M. & Puche, A. Unique neuronal tracers show migration and differentiation of SVZ progenitors in organotypic slices. *J. Neurobiol.* **49**, 326–338 (2001).
9. Carlén, M.*et al.* Functional integration of adult-born neurons. *Curr. Biol.* **12**, 606–608 (2002).
10. Petreanu, L. & Alvarez-Buylla, A. Maturation and death of adult-born olfactory bulb granule neurons: role of olfaction. *J. Neurosci.* **22**, 6106–6113 (2002).
11. Paton, J.A. & Nottebohm, F.N. Neurons generated in the adult brain are recruited into functional circuits. *Science* **225**, 1046–1048 (1984).
12. Shepherd, G.M. & Greer, C.A. Olfactory bulb. in *The Synaptic Organization of the Brain* (ed. Shepherd, G.M.) 159–203 (Oxford Univ. Press, New York, 1998).
13. Gheusi, G. *et al.* Importance of newly generated neurons in the adult olfactory bulb for odor discrimination. *Proc. Natl. Acad. Sci. USA* **97**, 1823–1828 (2000).
14. Cecchi, G.A., Petreanu, L.T., Alvarez-Buylla, A. & Magnasco, M.O. Unsupervised learning and adaptation in a model of adult neurogenesis. *J. Comput. Neurosci.* **11**, 175–182 (2001).
15. Okada, A., Lansford, R., Weimann, J.M., Fraser, S.E. & McConnell, S.K. Imaging cells in the developing nervous system with retrovirus expressing modified green fluorescent protein. *Exp. Neurol.* **156**, 394–406 (1999).
16. Lee, S.H., Lumelsky, N., Studer, L., Auerbach, J.M. & McKay, R.D. Efficient generation of midbrain and hindbrain neurons from mouse embryonic stem cells. *Nat. Biotechnol.* **18**, 675–679 (2000).
17. van Praag, H. *et al.* Functional neurogenesis in the adult hippocampus. *Nature* **415**, 1030–1034 (2002).
18. Song, H.J., Stevens, C.F. & Gage, F.H. Neural stem cells from adult hippocampus develop essential properties of functional CNS neurons. *Nat. Neurosci.* **5**, 438–445 (2002).
19. Liu, R.H., Morassutti, D.J., Whittemore, S.R., Sosnowski, J.S. & Magnuson, D.S. Electrophysiological properties of mitogen-expanded adult rat spinal cord and subventricular zone neural precursor cells. *Exp. Neurol.* **158**, 143–154 (1999).
20. Stewart, R.R., Zigova, T. & Luskin, M.B. K^+ currents in precursor cells isolated from the anterior subventricular zone of the neonatal rat forebrain. *J. Neurophysiol.* **81**, 95–102 (1999).
21. Castillo, P.E., Carleton, A., Vincent, J.D. & Lledo, P.-M. Multiple and opposing roles of cholinergic transmission in the main olfactory bulb. *J. Neurosci.* **19**, 9180–9191 (1999).
22. Nusser, Z., Kay, L.M., Laurent, G., Homanics, G.E. & Mody, I. Disruption of $GABA_A$ receptors on GABAergic interneurons leads to increased oscillatory power in the olfactory bulb network. *J. Neurophysiol.* **86**, 2823–2833 (2001).
23. Roy, N.S. *et al. In vitro* neurogenesis by progenitor cells isolated from the adult human hippocampus. *Nat. Med.* **6**, 271–277 (2000).
24. Stewart, R.R., Hoge, G.J., Zigova, T. & Luskin, M.B. Neural progenitor cells of the neonatal rat anterior SVZ express functional $GABA_A$ receptors. *J. Neurobiol.* **50**, 305–322 (2002).
25. Durand, G.M., Kovalchuk, Y. & Konnerth, A. Long-term potentiation and

functional synapse induction in developing hippocampus. *Nature* **381**, 71–75 (1996).
26. Komuro, H. & Rakic, P. Orchestration of neuronal migration by activity of ion channels, neurotransmitter receptors, and intracellular Ca^{2+} fluctuations. *J. Neurobiol.* **37**, 110–130 (1998).
27. Spigelman, I., Zhang, L. & Carlen, P.L. Patch-clamp study of postnatal development of CA1 neurons in rat hippocampal slices: membrane excitability and K^+ currents. *J. Neurophysiol.* **68**, 55–69 (1992).
28. Pirchio, M., Turner, J.P., Williams, S.R., Asprodini, E. & Crunelli, V. Postnatal development of membrane properties and delta oscillations in thalamocortical neurons of the cat dorsal lateral geniculate nucleus. *J. Neurosci.* **17**, 5428–5444 (1997).
29. Koestner, J. Membrane potential. in *Principles of Neural Science* (eds. Kandel, E.R., Schwartz, J.H. & Jessell T.H.) 81–94 (Elsevier, New York, 1991).
30. Tyzio, R. *et al.* The establishment of GABAergic and glutamatergic synapses on CA1 pyramidal neurons is sequential and correlates with the development of the apical dendrite. *J. Neurosci.* **19**, 10372–10382 (1999).
31. Khazipov, R. *et al.* Early development of neuronal activity in the primate hippocampus *in utero*. *J. Neurosci.* **21**, 9770–9781 (2001).
32. Cline, H.T. Dendritic arbor development and synaptogenesis. *Curr. Opin. Neurobiol.* **11**, 118–126 (2001).
33. Owens, D.F. & Kriegstein, A.J. Is there more to GABA than synaptic inhibition? *Nat. Rev. Neurosci.* **3**, 715–727 (2002).
34. Ben-Ari, Y. Excitatory actions of GABA during development: the nature of the nurture. *Nat. Rev. Neurosci.* **3**, 728–739 (2002).
35. Ganguly, K., Schinder, A.F., Wong, S.T. & Poo, M.M. GABA itself promotes the developmental switch of neuronal GABAergic responses from excitation to inhibition. *Cell* **105**, 521–532 (2001).
36. Alonso, G., Prieto, M. & Chauvet, N. Tangential migration of young neurons arising from the subventricular zone of adult rats is impaired by surgical lesions passing through their natural migratory pathway. *J. Comp. Neurol.* **405**, 508–528 (1999).
37. Lois, C., Garcia-Verdugo, J.M. & Alvarez-Buylla, A. Chain migration of neuronal precursors. *Science* **271**, 978–981 (1996).
38. Zhang, L.I. & Poo, M.M. Electrical activity and development of neural circuits. *Nat. Neurosci.* **4**, 1207–1214 (2001).
39. Snyder, J.S., Kee, N. & Wojtowicz, J.M. Effects of adult neurogenesis on synaptic plasticity in the rat dentate gyrus. *J. Neurophysiol.* **85**, 2423–2431 (2001).
40. Lemaire, V., Koehl, M., Le Moal, M. & Abrous, D.N. Prenatal stress produces learning deficits associated with an inhibition of neurogenesis in the hippocampus. *Proc. Natl. Acad. Sci. USA* **97**, 11032–11037 (2000).
41. Gould, E., Beylin, A., Tanapat, P., Reeves, A. & Shors, T.J. Learning enhances adult neurogenesis in the hippocampal formation. *Nat. Neurosci.* **2**, 260–265 (1999).
42. van Praag, H., Kempermann, G. & Gage, F.H. Running increases cell proliferation and neurogenesis in the adult mouse dentate gyrus. *Nat. Neurosci.* **2**, 266–270 (1999).
43. Rochefort, C., Gheusi, G., Vincent, J.D. & Lledo, P.-M. Enriched odor exposure increases the number of newborn neurons in the adult olfactory bulb and improves odor memory. *J. Neurosci.* **22**, 2679–2689 (2002).
44. Didier, A. *et al.* A dendro-dendritic reciprocal synapse provides a recurrent excitatory connection in the olfactory bulb. *Proc. Natl. Acad. Sci. USA* **98**, 6441–6446 (2001).
45. Walker, M.C., Ruiz, A. & Kullmann, D.M. Monosynaptic GABAergic signaling from dentate to CA3 with a pharmacological and physiological profile typical of mossy fiber synapses. *Neuron* **29**, 703–715 (2001).
46. Gutiérrez, R. Activity-dependent expression of simultaneous glutamatergic and GABAergic neurotransmission from the mossy fibers *in vitro*. *J. Neurophysiol.* **87**, 2562–2570 (2002).
47. Kanda, T., Sullivan, K.F. & Wahl, G.M. Histone–GFP fusion protein enables sensitive analysis of chromosome dynamics in living mammalian cells. *Curr. Biol.* **8**, 377–385 (1998).

© 2003 Nature Publishing Group http://www.nature.com/natureneuroscience